USE OF BEAM EMITTANCE MEASUREMENTS IN MATCHING PROBLEMS

J. Guyard*and M. Weiss

CERN, Geneva, Switzerland

Summary

The CERN new 50 MeV linac should operate with a computer-aided beam matching in which the transverse criteria are based on measured r.m.s. values of beam co-ordinates in phase space.

The collected data, however, need to undergo an intermediate treatment before significant results can be obtained and then used in computations. Some examples from the experimental study programme are given and the rôle of automated beam emittance measurements in matching problems discussed.

Introduction

The matching of a beam to a linear accelerator is a problem to be treated in the six-dimensional phase space. The usual simplification of this problem consists in decomposing the phase space into individual phase planes, which are then treated independently. Such a procedure is rigorously justified if the external and beam self forces are linear; it is still approximately valid if non-linear space-charge distributions, but of ellipsoidal type, are present and if one concentrates only on the analysis of r.m.s. beam coordinates in phase planes [1].

The matching conditions to the linac are defined for each phase plane and the quality of matching can be expressed in an identical way for the transverse and longitudinal beam dynamics. There is nevertheless a difference between transverse and longitudinal phase planes: for the former the beam emittance can be measured, whilst for the latter only the bunch longitudinal density distribution is usually checked. In compensation, the evolution of the longitudinal beam emittance in the linac is smoother, i.e. the wiggles of the longitudinal envelope around the mean one are small.

In this paper we concentrate on the problem of the transverse matching: assuming that the linac matching conditions are precisely known (which in fact is not the case), we analyse the usefulness of the measured beam parameters (which are affected by inevitable measurement errors) in view of a pre-computed matching. This analysis comes chronologically after some emittance measurements were carried out at 500 keV on our experimental set-up in the area of the 3 MeV linac model. The aim of these measurements has been to assess the validity of beam transport calculations by comparing them to the experimental results. Several difficulties have been encountered and their study was felt necessary before the start of measurements on the 750 keV beam transport system of the new CERN linac.

Results of measurements at 500 keV

The experimental study programme at 500 keV carried out in late 1974 and early 1975 dealt with various topics. In this paper we concentrate only on experiments treating the comparison between measurements and calculations.

The experimental set-up is shown schematically in Fig. 1. The emittance was measured at AP2 and AP3 in the classical way: the beam was sampled by a slit, AP2 or AP3 respectively (both of variable width) and the analysis of angles was made by a collector containing 48 nickel strips of 7 μm depth, deposited on a pyrex plate; the pitch was 0.5 mm. The slit AP1 was used to limit the beam if needed. The measurement was automated and the results displayed in graphic and numeric forms (Fig. 2). The graphs were used to judge the amount of distortions or presence of "non-protons" in the beam and the numerical values (indicating the first and second momenta of the distribution) were compared to those obtained by calculations.

The problem was in principle simple: measure the emittances at AP2, use results to transfer the beam by computations to AP3, compare calculations with measurements at AP3. The computations are based on r.m.s. values of beam coordinates in phase planes and assume an ellipsoidal density distribution in the beam. During the measurements, the beam intensity was maintained at rather low values in order to minimize the distortion of emittance ellipses.

In spite of the above precautions, a reasonable agreement between measurements and computations was found only after a careful check of possible measurement errors had been effected. In our case, the slit width was a major obstacle and in Fig. 3 we represent its influence on the size of the measured emittance. Only the introduction of the "significant emittance" (emittance obtained by extrapolating the slit width to zero) into the formulae permitted a relatively accurate determination of beam parameters α and β (see Tables 1 and 2).

The question which now logically arises is the following: how accurately do we in fact need to know the matching parameters α and β in order to achieve a proper matching and what precision can be expected from emittance measurements ?

Matching Criterion

In this chapter we derive a matching criterion for the beam entering the linear accelerator; this criterion will help us to assess the accuracy needed in the determination of α, β and γ. The linac matching parameters are calculated for an "equivalent beam", which has the same intensity and r.m.s. phase space coordinates as the actual beam, but is of a uniform density distribution in real space [2]. A beam is perfectly matched to a periodic structure if there are no betatron oscillations of its smooth envelope.

*) CERN Fellow, Université Nancy 1, Nancy, France.

A convenient matching criterion is therefore established in connection with the amount of residual oscillations of the mean beam envelope.

Suppose one has measured a beam and obtained

$$\gamma x^2 + 2\,\alpha xx' + \beta x'^2 = E$$

and that an ideal, matched beam of the same emittance is

$$\gamma_i x^2 + 2\,\alpha_i xx' + \beta_i x'^2 = E$$

(the meaning of the symbols is the usual one).

The ideal emittance is transformed into a circle $\eta^2 + \eta'^2 = E$ via the transformation

$$\begin{pmatrix}\eta\\ \eta'\end{pmatrix} = \begin{pmatrix}1/\sqrt{\beta_i} & 0\\ \alpha_i/\sqrt{\beta_i} & \sqrt{\beta_i}\end{pmatrix}\begin{pmatrix}x\\ x'\end{pmatrix} ,$$

while the "real" ellipse, with the same transformation, remains an ellipse:

$$\underbrace{\eta^2(\gamma\beta_i - 2\,\alpha\alpha_i + \frac{\beta}{\beta_i}\alpha_i^2)}_{G} + \underbrace{2\,\eta\eta'(\alpha - \frac{\beta}{\beta_i}\alpha_i)}_{A} + \underbrace{\eta'^2\frac{\beta}{\beta_i}}_{B} = E.$$

G, A, B are dimensionless parameters. It is convenient to define a mismatch factor by

$$M = \frac{R^2 - R_i^2}{R_i^2} = \frac{R^2}{E} - 1 ,$$

R being the major axis of the real emittance ellipse and R_i the radius of the ideal emittance circle (see Fig. 4). The relative residual betatron oscillations are derived from M by

$$\frac{\Delta R}{R_i} = \sqrt{1 + M} - 1 .$$

In eigenvector coordinates (ξ,ξ') the ellipse is in principal axes and has the equation

$$\frac{\xi^2}{(\sqrt{E/\lambda_1})^2} + \frac{\xi'^2}{(\sqrt{E/\lambda_2})^2} = 1$$

with λ_1,λ_2 as eigenvalues of its quadratic form. As $\lambda_1\lambda_2 = 1$, the major ellipse axis is given by

$$R^2 = \frac{E}{2}(B + G + \sqrt{(B+G)^2 - 4})$$

and the mismatch factor becomes:

$$M = \frac{1}{2}(B + G - 2 + \sqrt{(B+G)^2 - 4}) .$$

The expression for M can be written also as

$$M = \frac{1}{2}(B + G - 2 + \sqrt{(B+G-2)^2 + 4(B+G-2)})$$

and by calling $B + G - 2 = \Delta$, the mismatch factor is brought into the final form

$$M = \frac{1}{2}(\Delta + \sqrt{\Delta^2 + 4\Delta})$$

and becomes a function of the quantity Δ only. Both M and Δ are dimensionless. The function $M = f(\Delta)$ is presented on Fig. 5. For a perfect match, Δ and M are zero; the mismatch increases very rapidly with Δ. For example, if one wishes to have no more than 10% of smooth envelope oscillations in the linac, Δ must be < 0.05. In fact, Δ is the important quantity on which the matching depends and rather than expressing it through A, B and G, we shall define it by the measured and ideal matching parameters α, β, γ and α_i, β_i, γ_i respectively. After some algebraic operations, Δ can be brought in the most convenient form:

$$\Delta = (\alpha - \alpha_i)^2 - (\beta - \beta_i)(\gamma - \gamma_i) ,$$

where it depends only on differences $(\alpha - \alpha_i)$, $(\beta - \beta_i)$ and $(\gamma - \gamma_i)$, of which it is a quadratic function. In spite of the minus sign in the formula, it can be shown that Δ is always positive and becomes zero only for $\alpha = \alpha_i$, $\beta = \beta_i$, $\gamma = \gamma_i$.

The situation becomes complicated when the determination of α, β and γ is affected with errors and we actually measure $\alpha' = \alpha + \delta\alpha$, $\beta' = \beta + \delta\beta$ and $\gamma' = \gamma + \delta\gamma$. In order to match the beam, we will in such a case try to annul the expression:

$$\Delta' = (\alpha' - \alpha_i)^2 - (\beta' - \beta_i)(\gamma' - \gamma_i) ,$$

but in fact will be left with an error

$$\delta\Delta = \delta\beta\delta\gamma - (\delta\alpha)^2 ,$$

or written as the usual upper limit

$$\delta\Delta \leqslant |\delta\beta\delta\gamma| + (\delta\alpha)^2 .$$

This last expression gives in some cases very unrealistic results due to the fact that only two of the three parameters are independent.

If we wish to keep $\delta\Delta < 0.05$, which is a rather severe requirement, we must know more about measurement errors and therefore we shall analyse them in some detail in the next section.

Analysis of the emittance measurement

This analysis is carried out in two steps: first the systematic errors are studied and the importance of various factors assessed; then a simulation of the emittance measurement is done in order to get some numerical results.

Systematic measurement errors

These errors arise either from the imperfections of the measuring device, slit and collector, or from the action of space charge. The analysis presented here is to a certain extent inspired by[3,4] :

SLIT: the finite slit width influences the beam charge distribution falling on the collector. A

"point" source P_0 in the slit (corresponding to "zero" slit width) produces on the collector a distribution

$$f(x') = A\left(1 - \frac{x'^2}{a^2}\right) \qquad -a \leq x' \leq +a$$

$x' = y - y_0$ (see Fig. 6).

If the slit has a finite width 2d, we get on the same spot of the collector also distributions coming from other points in the slit satisfying the relations

$$f(x',x) = A\left(1 - \frac{(x' - x)^2}{a^2}\right) \qquad \begin{matrix} -d \leq x \leq d \\ -a+x \leq x' \leq a+x \end{matrix} .$$

It is assumed that the amplitude A stays the same for all emitting points in the slit. All the points in the slit give finally the collected distribution (see Fig. 6) obtained by integration

$$f_m(x') = \begin{cases} \int_{x_i}^{x_s} f(x,x')dx & \text{if } x_i < x_s \\ 0 & \text{if } x_i \geq x_s \end{cases}$$

with $\begin{cases} x_s = \text{MIN}[d, (x'+a)] \\ x_i = \text{MAX}[-d, (x'-a)] . \end{cases}$

The following conclusions can be drawn:

a) the collected distribution (normalized) has a smaller amplitude than the real one:

$$f_m(0) = A\left(1 - \frac{d^2}{3a^2}\right) ;$$

the difference becomes negligible if $d << a\sqrt{3}$;

b) the extension of the collected distribution is increased and goes from $-(d+a)$ to $+(d+a)$; this requires to keep $d << a$. The conditions are more difficult to fulfil with slim, inclined emittances having small angular cross sections.

COLLECTOR: the distribution falling on the collector is sampled by a certain number of wires (see Fig. 7a). Hence, instead of determining the true second momentum

$$\overline{x'^2} = \frac{\int x'^2 i(x')dx'}{\int i(x')dx'} ,$$

we in fact measure

$$\overline{x'^2}_m = \frac{\sum_i x'^2_i \int_{x'_i-h}^{x'_i+h} i(x')dx'}{\sum_i \int_{x'_i-h}^{x'_i+h} i(x')dx'} .$$

To get an idea about the errors involved, we have represented on Fig. 7b errors coming from a discrete sampling of a parabola. When the number of sampling points drops below ten, the error increases rapidly; the size of the wire has a relatively small influence, hence it can be chosen so as to obtain good detectable signals.

SPACE CHARGE: the distribution falling on the collector is influenced by the action of space charge between the slit and the collector. This influence is minimized if the distance slit-collector is chosen as

$$D_{opt} = \sqrt{\frac{2}{kI_0}} ,$$

where $k = e/m\varepsilon_0 v^3$ and I_0 the average density in the beam. At 750 keV, a current of 300 mA, having a diameter of 30 mm would require

$$D_{opt} \approx 0.65 \text{ m.}$$

Simulation of emittance measurement

The analysis of measurement errors so far has been treated in one dimension. The measurement of the emittance is however a two-dimensional problem and the two dimensions have to be studied together. A suitable method is to simulate numerically an emittance measurement and determine in this way the second momenta of a distribution (for simplicity the first momenta are taken to be zero). From these values we can then deduce the matching parameters:

$$\alpha = -\frac{\overline{xx'}}{E_{rms}}, \qquad \beta = \frac{\overline{x^2}}{E_{rms}}, \qquad \gamma = \frac{\overline{x'^2}}{E_{rms}}$$

$$E_{rms} = \left[\overline{x^2}\,\overline{x'^2} - (\overline{xx'})^2\right]^{\frac{1}{2}} .$$

To simplify the simulation, we neglect the effect of the slit width and the space charge and concentrate on the very important sampling errors. If there is only a limited number of sampling points, the "measured" r.m.s. values can differ considerably from the true ones.

We have chosen for the sampling a mesh of size 1 mm x 1 mrad and we sample the beam at the nodes of the mesh. The density distribution in the beam is assumed to be a two-dimensional parabola (in the phase plane), which is a sufficiently realistic assumption to provide usable results and has the advantage of not extending to infinity as the gaussian does.

In Fig. 8 we show emittance shapes which have been studied. Due to the symmetry of the problem, the error in $\overline{x^2}$ for emittance (1) corresponds to the error in $\overline{x'^2}$ in emittance (3) and vice versa. In Table 3 the results of computations for some typical emittances are summarized in form of algebraic errors obtained by comparing sampled r.m.s. values to the "true", analytically determined ones. The emittance areas studied are supposed to be on the lower and upper limit of those expected in the new 750 keV beam transport.

The errors and in consequence the mismatch vary with the shape and size of the emittance. Best

results are obtained for bigger (more sampling points) and round emittances, other shapes being essentially equivalent (a certain spread is due to the statistical character of the sampling).

From the simulation calculations we have derived a practical, approximate rule for judging the feasibility of achieving a good matching via emittance measurements. Considering the ellipse of Fig. 9, we count the sampling points along the indicated segments PQ and RS and choose the segment with less samples. If N is the number of these samples, we have approximately:

N<5 : measurement errors big, the corresponding $\delta\Delta$ greater than 0.1; measurement not good enough for proper matching.

$5 \lesssim N \lesssim 10$: error in $\delta\Delta$ of the order of 0.1 to 0.01.

N >10 : errors negligible, $\delta\Delta$ < 0.01.

Conclusion

An analysis concerning the precision of emittance measurements has been carried out as a consequence of problems encountered in our beam studies at 500 keV. Systematic measurement errors have been reviewed and the importance of a proper sampling recognized. Sampling errors have been evaluated for some typical emittance shapes and sizes, by using a "sampling mesh" with a resolution similar to that of our emittance measuring device.

In our study, the real beam has always been idealized (no aberrations, ellipsoidal density distribution), as has been the emittance measurement (apart from sampling, no other errors). The results quoted have therefore to be taken with these restrictions and considered only as guiding indications. However, before treating a real beam (measurements at 750 keV are in course) it was felt that the matching problems concerning an ideal beam had to be solved.

Acknowledgement

The problems treated in this paper have been discussed with D.J. Warner, L. Marcé and recently with B. Schorr; we acknowledge the contribution of all of them.

References

1. F. Sacherer, RMS envelope equation with space charge, CERN/SI/Int. 70-12.
2. B. Bru and M. Weiss, Computational methods and computer programs for linearized analysis of periodic structures and beam transport systems under space-charge conditions, MPS/LIN/72-4.
3. L.R. Evans and D.J. Warner, A critical study of emittance measurements of intense low energy proton beams, MPS/LIN/72-1.
4. J. Guyard and L. Marcé, Paramètres significatifs d'un faisceau de protons à 500 keV issus de la mesure des moyennes quadratiques, CERN/MPS/LIN 75-1.

Table 1 : Emittances and α,β parameters extrapolated from measured values.

Series	I mA	E_H (rms) mm mrad	E_V (rms) mm mrad	AP2 Horizontal β mm/mrd	AP2 Horizontal $-\alpha$	AP2 Vertical β mm/mrd	AP2 Vertical $-\alpha$	AP3 Horizontal β mm/mrd	AP3 Horizontal $-\alpha$	AP3 Vertical β mm/mrd	AP3 Vertical $-\alpha$
A	20	1.6	1.8	18.9	14.9	14.2	12.1	41.7	24.1	34.6	22.4
B	10	2.9	3.1	4.7	4.3	4.1	4.0	11.0	7.2	11.3	8.5

Table 2 : Parameters obtained by beam transport computation.

AP3 Horizontal β mm/mrd	AP3 Horizontal $-\alpha$	AP3 Vertical β mm/mrd	AP3 Vertical $-\alpha$
42.0	26.1	33.3	21.9
11.6	8.0	10.6	7.6

Table 3 : Examples of computed errors and mismatch factors for some typical emittances.

	Shape and area of the ellipses: 1		2		4	
Phase area/π mm mrad	30	60	30	60	30	60
$\delta E_{rms}/E_{rms}$ [%]	15.6	-1.3	-7.6	2.1	0.7	0.2
$\delta\beta/\beta$ [%]	-26.2	2.0	10.8	-3.2	0.0	0.0
$\delta\alpha/\alpha$ [%]	18.9	-2.6	10.9	-3.3	9.1	4.4
$\delta\gamma/\gamma$ [%]	20.8	-2.1	10.8	-3.2	0.1	0.0
$\delta\Delta$	0.055	$<10^{-3}$	0.013	10^{-3}	$<10^{-3}$	$<10^{-3}$
M	0.263	0.021	0.122	0.033	6.10^{-3}	2.10^{-3}

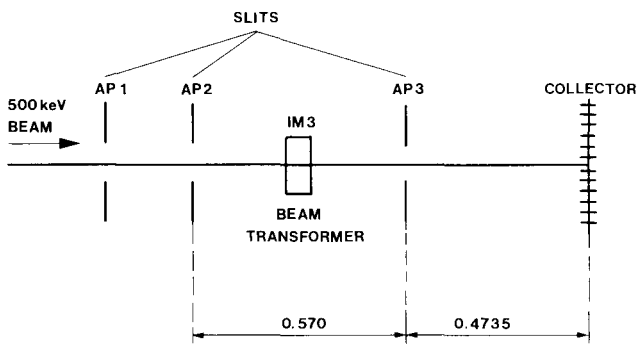

Fig. 1 : Experimental set-up

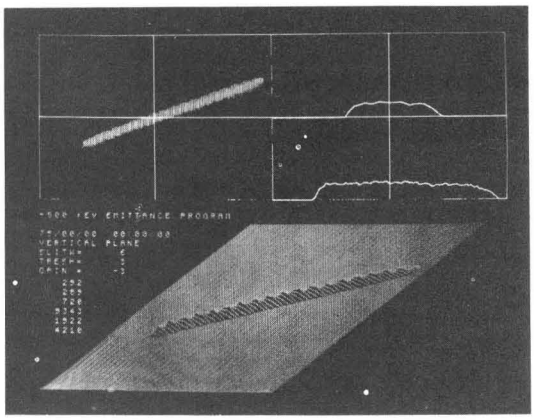

Fig. 2 : Display of a measured emittance

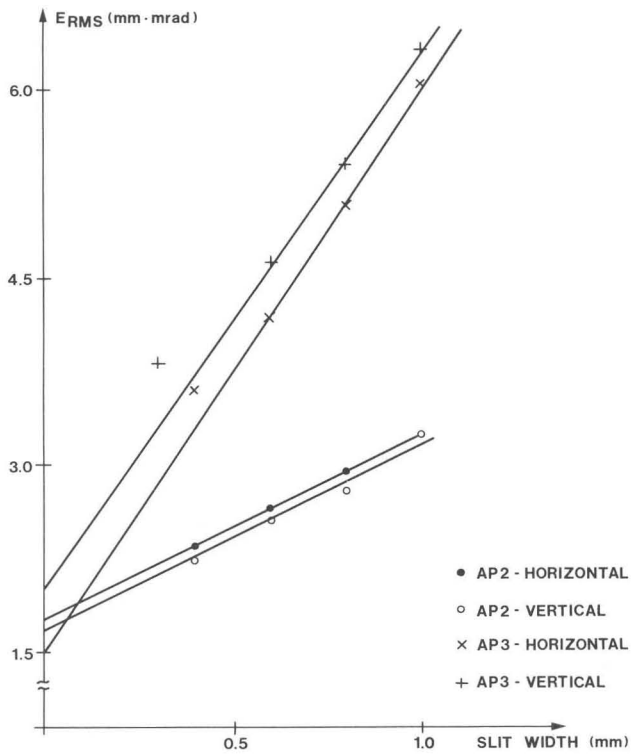

Fig. 3 : RMS emittance as function of slit width

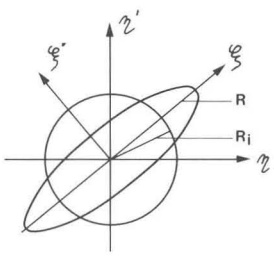

Fig. 4 :
Transformed ideal
and real emittances

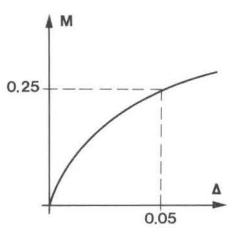

Fig. 5 :
Function M = F(Δ)

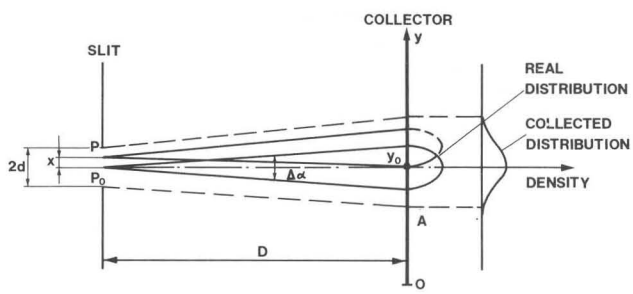

Fig. 6 : Influence of slit width on collected densities

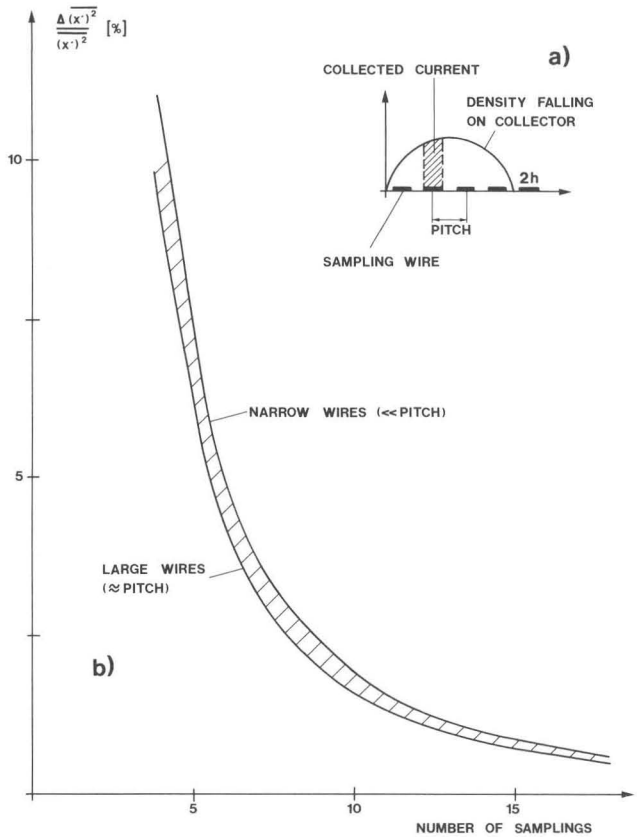

Fig. 7 : a) Sampling with the collector
b) Errors as function of the number of samplings

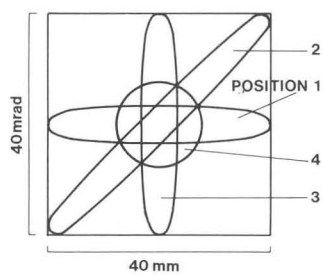

Fig. 8 :
Typical emittance shapes
used in the simulation

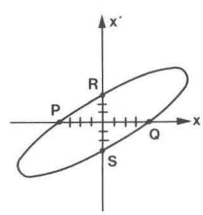

Fig. 9 :
Characteristic segments
for the two-dimensional
sampling